CHALMERS
UNIVERSITY OF TECHNOLOGY

DDM-Based Accurate and Efficient RIS Modeling for Over-the-Air Mutual Coupling Analysis and Comparison vs Macromodeling

Citation for the original published paper (version of record):
Ghaderi Aram, M., Svensson, T., Maxharraj, F. et al (2026). DDM-Based Accurate and Efficient RIS Modeling for Over-the-Air Mutual Coupling Analysis and
Comparison vs Macromodeling. IEEE Open Journal of Antennas and Propagation, In Press.
http://dx.doi.org/10.1109/OJAP.2026.3695418

IEEE Open Journal of Antennas and Propagation

Received 25 Feb., 2026; revised 23 April, 2026; accepted 17 May, 2026.

Digital Object Identifier 10.1109/OJAP.2026.3695418

DDM-Based Accurate and Efficient RIS Modeling for Over-the-Air Mutual Coupling Analysis and Comparison vs Macromodeling

MORTEZA GHADERI ARAM* (Graduate Student Member, IEEE), TOMMY SVENSSON* (Senior Member, IEEE), FITIM MAXHARRAJ* (Graduate Student Member, IEEE), AND ROB MAASKANT* (Senior Member, IEEE)

[1*]Department of Electrical Engineering, Chalmers University of Technology, Gothenburg, Sweden

CORRESPONDING AUTHOR: Morteza Ghaderi Aram (e-mail: aramg@chalmers.se).

ABSTRACT Existing modeling approaches for reconfigurable intelligent surfaces (RISs)—including scalar approximations, boundary-condition-based formulations, and conventional full-wave solvers—either lack accuracy in capturing aperiodic interactions or become computationally prohibitive for electrically large, multi-scale structures. To address these limitations at least for a certain class of RISs, which are composed of open-cavity-based meta-atoms, this paper presents a rigorous and computationally efficient hybrid domain decomposition method (H-DDM). The method decomposes each meta-atom into interior and exterior subproblems, enabling fast and accurate modeling of over-the-air mutual coupling effects while preserving microscopic field behavior. The proposed H-DDM is cross-validated against CST full-wave solvers and compared against two widely used approximate methods: macromodeling (MM) and the element-in-array-pattern (EIAP) technique. Using RIS panels of varying sizes which are beamformed to have a non-specular reflection under a normal plane wave incidence, we demonstrate that H-DDM achieves very good agreement with full-wave reference solutions, while MM and EIAP exhibit increasing deviations in sidelobe regions due to their inherent assumptions. The results confirm that H-DDM provides a powerful and reliable tool for analyzing open-cavity based RIS panels and offers a promising pathway toward fast, high-fidelity EM modeling of next-generation beamforming metasurfaces.

INDEX TERMS Metasurfaces, Surrogate Model, Domain Decomposition Technique, RIS

I. INTRODUCTION

METAMATERIALS and their 2D counterparts, metasurfaces (MTSs) [1], which consist of subwavelength units and exhibit extraordinary properties not found in nature, have recently received a surge of interest in their simulation, design, and optimization. A representative example of their real-world engineering realization is the concept of reconfigurable intelligent surfaces (RISs) [2]–[4], which has arguably been one of the research hotspots in both the electromagnetic (EM) and wireless communities during recent years. Belonging to the category of electrically large EM problems, RISs which typically consist of multi-scale components are in urgent need of an efficient full-wave (FW) simulation and/or optimization toolbox tailored to their quasi-periodic structures.

Generally speaking, all the RIS analysis methods proposed in the literature to address the challenge can be classified into three main categories [5]: (1) scalar approximation, (2) boundary-condition-based methods, and (3) computational electromagnetic methods, as follows in further detail. Assuming MTS units as point scatterers, the scalar approximation method is the first category that resembles the antenna array factor (AF) theory and has been widely used in the design and optimization of RISs [6], [7]. Plus, low-cost surrogate models based on equivalent circuit (EC) [8] and microwave network [9], [10] theories can also be associated with this approximate solution family and, in fact, fit well

This work is licensed under a Creative Commons Attribution 4.0 License. For more information, see https://creativecommons.org/licenses/by/4.0/

into the framework of AF theory. While providing fast approximate solutions, methods in this category exhibit limited accuracy and do not account for aperiodic interactions, which occur in reality as mutual coupling among a disordered juxtaposition of meta-atoms.

The second category treats MTSs as polarizing discontinuities with zero thickness and thus models them as boundary conditions (BCs), either in the form of impedance BC [11] or generalized sheet transition condition (GSTC) [12]. Methods in this well-established category avoid ill-conditioned problems and hence considerably reduce the computational burden of the analysis, but they are based on the local periodicity assumption, can only handle single-layer structures, and usually ignore the normal susceptibility components at the interface.

The third category, consisting of such conventional computational electromagnetic methods (CEMs) as finite element method (FEM) [13] and integral-equation-based (IE-based) method of moment (MoM) [14], provides rigorous solutions and remains essential in simulating complex metamaterials, especially when it is crucial to capture the microscopic fields within each MTS resonator and/or their higher-order modes. Moreover, the domain decomposition method (DDM), which allows for dividing MTS panels into subdomains while still preserving the interactions among meta-atoms, naturally lends itself to the hybridization of FEM and IE and has already been investigated in the framework of finite element-boundary element- domain decomposition method (FEM-BEM-DDM) [5]. Specifically, Jiang et al. [5] have used FEM to analyze sensitive internal structures with relatively high mesh resolution, ensured field continuity while stitching the non-conformal FEM-BEM meshed regions at the interface, and afterwards used BEM with a much coarser mesh density to predict the far-field (FF) scattering pattern in the exterior region. They have applied the technique to a comprehensive range of metamaterials, both in scattering and radiation paradigms, from a frequency selective surface (FSS) to an artificial magnetic conductor (AMC) and also a lens-array beamforming metasurface. However, their use of in-house developed FEM to handle interior domains remains restricted to the so-called 'frozen coding patterns' and does not include lumped-element-based dynamic tunability.

This study, which is an extension of the authors' work originally presented at ICEAA-IEEE APWC 2025 [15], bears some similarity to [5], in the sense that it proposes a hybrid rigorous method for simulations of metamaterials. Compared to [5], the distinction, however, is that the IE solver of a commercial software package (CST Microwave Studio Suite®), instead of an in-house developed FEM, is used in our study to allow for handling all sorts of interior domains, including the sophisticated ones with embedded lumped elements. In other words, and to be in line with the acronym FEM-BEM-DDM defined in [5], our proposed method can be considered as CST-MoM-DDM, which we just refer to as hybrid DDM (H-DDM) for short hereafter. Therefore, the first contribution of this study is to introduce a novel hybrid IE-DDM technique for analyzing a certain class of metasurface beamforming panels. Although this technique limits practical realizations to open-cavity based structures only and is therefore best applicable to over-the-air coupling scenarios, it proves to have major computational advantages and paves the way for further characterization of this family of beamforming panels. Furthermore, the proposed technique is cross-validated with FW analyses and also compared in terms of accuracy versus Macromodeling (MM) [9], a local-periodicity-based surrogate modeling technique from the literature. The second follow-up contribution of the work is then to utilize the developed H-DDM in the framework of element-in-array pattern (EIAP) analysis [16], [17] to study over-the-air mutual coupling effects in beamformed panels with different sizes.

The remainder of the paper is organized as follows. The problem formulation and mathematical background of H-DDM, along with a summary of the algorithms taken from the literature for comparison, are provided in Section II. Section III presents the numerical results of simulating several beamforming panels using these algorithms, followed by a brief discussion on the accuracy and limitations of each method. Concluding remarks and directions for future studies are finally presented in Section IV.

II. MODELING METHODS

It is a common practice in the design of metasurfaces to use perfect electric conductor (PEC) baffles, either in the form of substrate integrated waveguide (SIW) vias [2] or a solid metallic septum [18], in order to suppress the inter-element cross-talks at the substrate level among meta-atoms. While this may come at a cost of added manufacturing complexity, the encagement of unit cells with PEC walls can open up other possibilities from analytical point of view by allowing us to revisit Harrington's original work [19] on aperture problems where the application of method of moment (MoM) to the integral field equations (EFIEs & MFIEs) leads to the concept of generalized admittance matrix. In particular, these types of reflective, open-cavity based RIS panels can be cast into the domain decomposition framework of Fig. 1 by considering it at each individual unit cell level as a cavity-to-exterior space coupling problem in which EM energy couples only between two regions of space which are isolated except for one aperture. In accord with this line of reasoning, we adopt a cavity-based unit cell with varactor tunability, whose geometric details are described in Section III.

A. HYBRID DOMAIN DECOMPOSITION METHOD

Summarizing our recently published DDM framework [15], Fig. 1 shows the underlying concept behind the method in conjunction with Love's equivalence theorem which results in both magnetic and electric surface current densities $\boldsymbol{M}_s$ and $\boldsymbol{J}_s^a$, $\boldsymbol{J}_s^b$. This leads to a formulation based on a magnetic

This article has been accepted for publication in IEEE Open Journal of Antennas and Propagation. This is the author's version which has not been fully edited and content may change prior to final publication. Citation information: DOI 10.1109/OJAP.2026.3695418

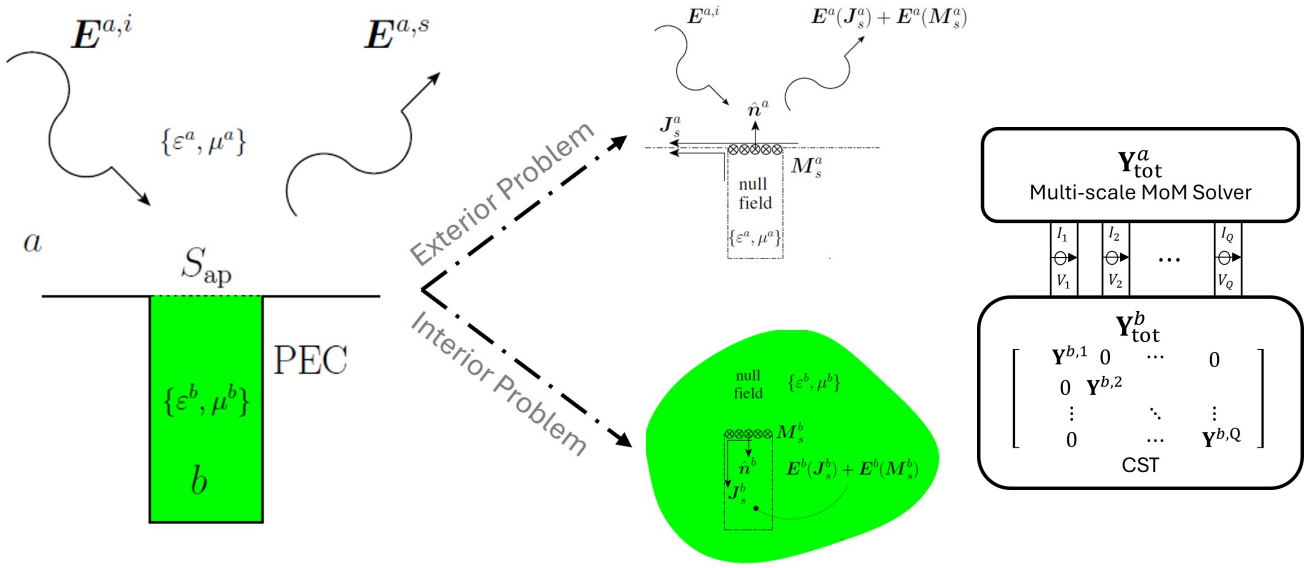

(a) (b)

FIGURE 1. The conceptual idea behind DDM at (a) the unit cell level where the original scattering problem is decomposed into interior equivalent fields in region b and exterior equivalent fields in region a and (b) at the panel level where the generalized admittance matrix concept [19] is cast into a MoM-based DDM framework [15].

field integral equation (MFIE) and two electric field integral equations (EFIEs) as further revealed below. Note that the normal unit vectors to the aperture surface S_{ap} for two equivalent internal and external regions (labeled as b and a, respectively) are set to point in opposite directions in the figure. In other words, $\hat{\boldsymbol{n}}^a = -\hat{\boldsymbol{n}}^b$ and since the tangential electric field component across the surface should remain continuous, one can conclude that $\hat{\boldsymbol{n}}^a \times \boldsymbol{M}_s^a = -\hat{\boldsymbol{n}}^a \times \boldsymbol{M}_s^b$, i.e. there exists a single magnetic surface current $\boldsymbol{M}_s^a = -\boldsymbol{M}_s^b = \boldsymbol{M}_s$ for the two regions. As emphasized in the figure, the interior electric surface current $\boldsymbol{J}_s^b$ is, however, different from the exterior electric surface current $\boldsymbol{J}_s^a$, essentially leading to the existence of two distinct EFIEs later on.

The MFIE formulation, whose derivation can be found in the Appendix, begins by enforcing continuity of tangential magnetic fields across the aperture, i.e. $\boldsymbol{H}_{\text{tan}}^a = \boldsymbol{H}_{\text{tan}}^b$, and can be cast into the framework of MoM and Galerkin weighted residual approach by expanding the surface currents in terms of RWG basis functions [20] $\{\boldsymbol{m}_n,\ \boldsymbol{i}_n^a,\ \boldsymbol{i}_n^b\}$ as follows

$$\boldsymbol{M}_s(\boldsymbol{r}) = \sum_{n=1}^{N} V_n \boldsymbol{m}_n(\boldsymbol{r}), \qquad \text{for} \quad \boldsymbol{r} \in S_{\text{ap}} \tag{1}$$

$$\boldsymbol{J}_s^a(\boldsymbol{r}) = \sum_{n=1}^{N^a} I_n^a \boldsymbol{i}_n^a(\boldsymbol{r}), \quad \boldsymbol{J}_s^b(\boldsymbol{r}) = \sum_{n=1}^{N^b} I_n^b \boldsymbol{i}_n^b(\boldsymbol{r}), \tag{2}$$

where N is the number of expanding sub-domain basis functions for $\boldsymbol{M}_s$ and $\mathbf{V} = [V_1, V_2, \cdots, V_N]^T$ is the vector of unknown coefficients to be determined as the ultimate goal of solving the DDM equations, while $\mathbf{I}^a = [I_1^a, I_2^a, \cdots, I_{N^a}^a]^T$ and $\mathbf{I}^b = [I_1^b, I_2^b, \cdots, I_{N^b}^b]^T$ are dependent variables and can be conveniently found once $\mathbf{V}$ is solved for. By applying the standard Galerkin testing procedure (explained in more detail in the Appendix), defining the aperture admittances for each region as $\langle -\boldsymbol{m}_m, \boldsymbol{H}_{\text{tan}}^{a,b}(\boldsymbol{m}_n)\rangle = Y_{mn}^{a,b}$, and setting $\langle \boldsymbol{m}_m, \boldsymbol{H}_{\text{tan}}^{a,i}\rangle$ and $\langle \boldsymbol{m}_m, \boldsymbol{H}_{\text{tan}}^{b,i}\rangle$ equal to $I_m^{a,i}$ and $I_m^{b,i}$, respectively, we obtain a set of N linear equations which can then be conveniently represented in the following compact vector-matrix multiplication form:

$$\left[\mathbf{Y}^a + \mathbf{Y}^b\right]\mathbf{V} + \mathbf{C}^b\mathbf{I}^b - \mathbf{C}^a\mathbf{I}^a = \mathbf{I}^{a,i} - \mathbf{I}^{b,i}. \tag{3}$$

where $C_{mn}^{a,b} = \langle \boldsymbol{m}_m, \boldsymbol{H}_{\text{tan}}^{a,b}(\boldsymbol{i}_n^{a,b})\rangle$. As stated before, the ultimate goal is to find $\boldsymbol{M}_s$ of which $\mathbf{V}$ is an N-term variational approximate solution. In fact, $\mathbf{I}^a$ and $\mathbf{I}^b$ are intermediate, dependent variables and can therefore be expressed in terms of $\mathbf{V}$ by enforcing the second set of boundary conditions, i.e. ensuring electric field continuity which results in the following two EFIEs:

$$\mathbf{Z}^a\mathbf{I}^a = \mathbf{D}^a\mathbf{V} + \mathbf{V}^{a,i} \tag{4}$$

$$\mathbf{Z}^b\mathbf{I}^b = -\mathbf{D}^b\mathbf{V} + \mathbf{V}^{b,i}, \tag{5}$$

where

$$Z_{mn}^{a,b} = -\langle \boldsymbol{i}_m^{a,b}, \boldsymbol{E}_{\text{tan}}^{a,b}(\boldsymbol{i}_n^{a,b})\rangle \tag{6}$$

$$D_{mn}^{a,b} = \langle \boldsymbol{i}_m^{a,b}, \boldsymbol{E}_{\text{tan}}^{a,b}(\boldsymbol{m}_n) - \hat{\boldsymbol{n}}^{a,b} \times \boldsymbol{m}_n\rangle \tag{7}$$

$$V_m^{a,i} = \langle \boldsymbol{i}_m^a, \boldsymbol{E}_{\text{tan}}^{a,i}\rangle, \quad V_m^{b,i} = \langle \boldsymbol{i}_m^b, \boldsymbol{E}_{\text{tan}}^{b,i}\rangle. \tag{8}$$

Finally, by rearranging the above equations and substituting $\mathbf{I}^a$ and $\mathbf{I}^b$ back into Equation (3), we obtain the final generalized admittance formula as:

$$\left[\mathbf{Y}_{\text{tot}}^a + \mathbf{Y}_{\text{tot}}^b\right]\mathbf{V} = \mathbf{I}, \tag{9}$$

where

$$\mathbf{Y}^a_{\text{tot}} = \mathbf{Y}^a - \mathbf{C}^a(\mathbf{Z}^a)^{-1}\mathbf{D}^a \tag{10a}$$

$$\mathbf{Y}^b_{\text{tot}} = \mathbf{Y}^b - \mathbf{C}^b(\mathbf{Z}^b)^{-1}\mathbf{D}^b \tag{10b}$$

$$\mathbf{I} = \left[\mathbf{I}^{a,i} + \mathbf{C}^a(\mathbf{Z}^a)^{-1}\mathbf{V}^{a,i}\right] - \left[\mathbf{I}^{b,i} + \mathbf{C}^b(\mathbf{Z}^b)^{-1}\mathbf{V}^{b,i}\right]. \tag{10c}$$

Once $\mathbf{V}$ is known from solving Eq. (9), one can obtain $\mathbf{I}^a$ and $\mathbf{I}^b$ from Eqs. (4) and (5) and then find the magnetic surface current distribution through RWG basis function expansion of Eq. (1) as well as the electric surface current distributions using Eq. (2). Having $\boldsymbol{M}_s$ and $\boldsymbol{J}^a_s$ at hand, the scattered field from the panel in region a can then be easily calculated as $\boldsymbol{E}^a(\boldsymbol{M}_s) + \boldsymbol{E}^a(\boldsymbol{J}^a_s)$ using the operator relations which are explicitly expressed in terms of the scalar Green's function of each region in the Appendix.

Equipped with the developed DDM methodology above, we can now proceed to extend the method to all sorts of open-cavity based beamforming panels, including reconfigurable ones that may have lumped circuit elements such as Varactor or PIN diodes embedded in their interior region. To this end, we interface the above method with CST and propose a hybrid CST-MoM-DDM framework called hybrid DDM (H-DDM) henceforth. As for the interior domain, $\mathbf{Y}^b_{\text{tot}}$ can be conveniently computed using CST, allowing for the analysis of complex cells having highly inhomogeneous material distributions. This hybrid method essentially replaces the MoM-based calculation in (10b) by the numerical calculation per aperture type through a plane wave (PW) characterization scheme in CST as summarized below:

- Each unique unit cell type, based on its geometry or reflection configuration, is characterized as a single isolated reflectarray element in CST by letting a plane wave be normally incident while monitoring the total aperture E- and H-fields. Let these fields for unit cell q be $\boldsymbol{E}^q$ and $\boldsymbol{H}^q$ defined over the aperture S^q_{ap}.
- From $\boldsymbol{E}^q$ and $\boldsymbol{H}^q$, one can determine the aperture admittance looking into the interior unit cell [21, see e.g. Fig. 3-12], for unit cell q: $Y^{b,q} = \iint_{S^q_{\text{ap}}} [\boldsymbol{E}^q \times \boldsymbol{H}^q] \cdot \hat{\boldsymbol{n}}^b \mathrm{d}S$. Introducing the magnetic current $\boldsymbol{M}^q = \hat{\boldsymbol{n}}^b \times \boldsymbol{E}^q$, this integral can also be written as $Y^{b,q} = \iint_{S^q_{\text{ap}}} \boldsymbol{M}^q \cdot \boldsymbol{H}^q \mathrm{d}S$ for non-normalized aperture fields [22].
- The diagonal matrix $\mathbf{Y}^b_{\text{tot}}$ is constructed by replicating the corresponding $Y^{b,q}$ along its diagonal from the few uniquely calculated aperture admittances.
- One now has single-mode (non-normalized) aperture mode currents $\boldsymbol{M}^q$ for aperture $q = 1, 2, \ldots, Q$. Let the corresponding basis function expansion coefficient vector be denoted as $\mathbf{V}^q$. Stacking these into the block diagonal matrix $\mathbf{V}_{\text{CBF}} = \text{blkdiag}(\mathbf{V}_1, \mathbf{V}_2, \ldots, \mathbf{V}_Q)$, we can now compress and solve Eq. (9) as $\left[\mathbf{V}^{\text{T}}_{\text{CBF}}\mathbf{Y}^a_{\text{tot}}\mathbf{V}_{\text{CBF}} + \mathbf{Y}^b_{\text{tot}}\right]\mathbf{V}_{\text{red}} = \mathbf{V}^{\text{T}}_{\text{CBF}}\mathbf{I}$.
- After solving for $\mathbf{V}_{\text{red}}$, one can find the solution for the magnetic current in (9) as $\mathbf{V} = \mathbf{V}_{\text{CBF}}\mathbf{V}_{\text{red}}$.

Note that while the exact DDM formulation presented at the beginning of this section employs a full RWG expansion for the aperture magnetic current, the subsequent development of CST-based hybridization compresses each physical aperture into a single state-specific characteristic basis function (CBF) obtained from isolated-cell aperture fields. Mutual coupling is still accounted for through the reduced exterior matrix $\mathbf{V}^{\text{T}}_{\text{CBF}}\mathbf{Y}^a_{\text{tot}}\mathbf{V}_{\text{CBF}}$, but each local aperture current is restricted to a one-dimensional subspace, i.e., only its complex amplitude is solved for while its spatial profile is assumed fixed. For the PEC-walled open-cavity unit cells and normal-incidence beamforming cases considered here, comparison with CST indicates that this approximation is sufficiently accurate. Its limitation is that scenarios involving higher-order aperture or cavity modes, weaker confinement, or strong coupling-induced field reshaping may require a richer local basis; considering multiple CBFs per aperture and assessing the associated accuracy–efficiency trade-off is left for future work.

B. MACROMODELING

Macromodeling (MM), which builds upon microwave network theory, is an efficient technique for fast prediction of the reflection property and far-field (FF) pattern of RISs [9]. Allowing for a separate design of the passive structure and the tunable devices, MM can also be used in the design phase of a meta-atom [10]. Following a similar procedure as in the original study [9], we start the MM analysis by referring to Fig. 2a, where the simulation setup of the passive structure of the meta-atom under periodic boundary conditions (PBC) is composed of a Floquet port (denoted as port 1) and a lumped port inside the waveguide cavity (denoted as port 2). The rest of the steps taken during the analysis can be briefly itemized below:

- We first model the lumped element varactor diode as a voltage-controlled capacitor (C_v) that can cover the range of $[0.05 - 6]$ pF, thus the load impedance in Fig. 2b can be expressed as $Z_L(\omega) = -j/C_v\omega$.
- Next, we treat the meta-atom as a passive two-port network by replacing the varactor with a lumped port (port 2 in Fig. 2a). This allows for a fast and efficient calculation of the two-port S-matrix or equivalently Z-matrix ($\mathbf{Z}_p$) of the passive structure using a full-wave analyzer such as CST.
- Having $\mathbf{Z}_p$ at hand and by performing the standard network analysis depicted in Fig. 2b, one can then easily calculate the local reflection coefficient at the interface of meta-atom with input impedance Z_{Meta} and air with the intrinsic impedance η_0 for different frequencies and under different varactor loadings as

follows:

$$\Gamma(\omega) = \frac{Z_{\text{Meta}}(\omega) - \eta_0}{Z_{\text{Meta}}(\omega) + \eta_0}; \tag{11}$$

$$Z_{\text{Meta}}(\omega) = Z_{11}(\omega) - \frac{Z_{12}(\omega)Z_{21}(\omega)}{Z_L(\omega) + Z_{22}(\omega)}\ . \tag{12}$$

- Finally, linearly polarized θ-component of the FF-pattern $F(\theta,\phi)$ and directivity $\text{Dir}(\theta,\phi)$ of the RIS panel, which is typically a rectangular grid of meta-atoms arranged in N columns and M rows, can be calculated using the pattern multiplication rule and the conventional array factor concept [23]. To this end, one needs to loop through all the meta-atom elements in the RIS panel, calculate the amplitude $|\Gamma_{mn}|$ and phase $\angle\Gamma_{mn}$ of the local reflection coefficient of each cell as stated above in Eq. (11), and incorporate the element pattern of one isolated meta-atom $G(\theta,\phi)$ as follows:

$$F(\theta,\phi) = G(\theta,\phi)\sum_{m=1}^{M}\sum_{n=1}^{N}|\Gamma_{mn}|e^{-j\left(\boldsymbol{k}\cdot\boldsymbol{r}_{mn}+\angle\Gamma_{mn}\right)}; \tag{13}$$

$$\text{Dir}(\theta,\phi) = \frac{4\pi|F(\theta,\phi)|^2}{\int_0^{2\pi}\int_0^{\pi}|F(\theta,\phi)|^2\sin\theta d\theta d\phi}, \tag{14}$$

where $\boldsymbol{k} = k\sin\theta\cos\phi\hat{x} + k\sin\theta\sin\phi\hat{y}$ with k as the free-space wavenumber, $\boldsymbol{r}_{mn} = (n-1)d_x\hat{x} + (m-1)d_y\hat{y}$, and θ, ϕ, d_x, and d_y are the angles of elevation, azimuth, inter-element spacings in x and y, respectively.

C. ELEMENT-IN-ARRAY PATTERN

For FF-pattern analysis of large-scale RISs, it can be highly efficient to introduce an approximate method, wherein the scattering problem of the entire panel can be divided into a superposition of a series of small-scale subarrays. Previous studies reported in [16] and [17] have utilized this concept of subarrays to investigate the mutual coupling impact in reflectarray and RIS designs, respectively. For a panel consisting of $Q = M \times N$ total elements, they considered 1D and 2D subarrays in the form of an S-element overlapping/gliding convolutional window with $1 \le S \le Q$, where the two extremes of 1 and Q are the isolated element summation and the whole panel analysis at once, respectively. Their conclusion and findings were that the immediate surrounding neighbors to the central element within each subarray have the highest contribution to the mutual coupling effect and that the size of the subarray can be practically kept small relative to the size of the entire panel. Dubbed as "element-in-array-pattern" (EIAP) in [16], this simple technique expresses the total scattered far electric field as $\boldsymbol{E}_{\text{tot}} = \sum_{n=1}^{N_{\text{SA}}}\boldsymbol{E}_n(\theta,\phi)$ where N_{SA} is the total number of subarrays and $\boldsymbol{E}_n$ is the scattered field by subarray n (i.e. an S-element gliding window centered on the nth cell).

In this study, we adopted EIAP in order to investigate the extent to which a complete overlook of the potential over-the-air mutual couplings among the cells can distort the final prediction of the scattering pattern of RIS panels with different sizes. Therefore, only a 1-element window EIAP analysis is conducted here, which automatically implies $N_{\text{SA}} = Q$ and can be easily incorporated into the H-DDM framework introduced in Section II-A. Similar to the original H-DDM formulation, the block-diagonal admittance matrix of the interior domain $\mathbf{Y}^b_{\text{tot}}$ remains the same here, reiterating that there is no internal cross-talk at the substrate level of the panel due to utilization of the interior cavity walls. However, unlike the original H-DDM, depicted in Fig. 1b, which considers a fully populated exterior admittance matrix $\mathbf{Y}^a_{\text{tot}}$ to account for all over-the-air mutual couplings, 1-element EIAP considers a diagonalized $\widetilde{\mathbf{Y}}^a_{\text{tot}}$ for the exterior region as well, hence neglecting all over-the-air cross-talks among adjacent cells. In other words, this isolated-element implementation of EIAP involves solving a series of Q H-DDM problems iteratively, one at a time, and superimposing them in the end to yield the total far-field scattering pattern of the entire panel, as schematically explained in Fig. 3.

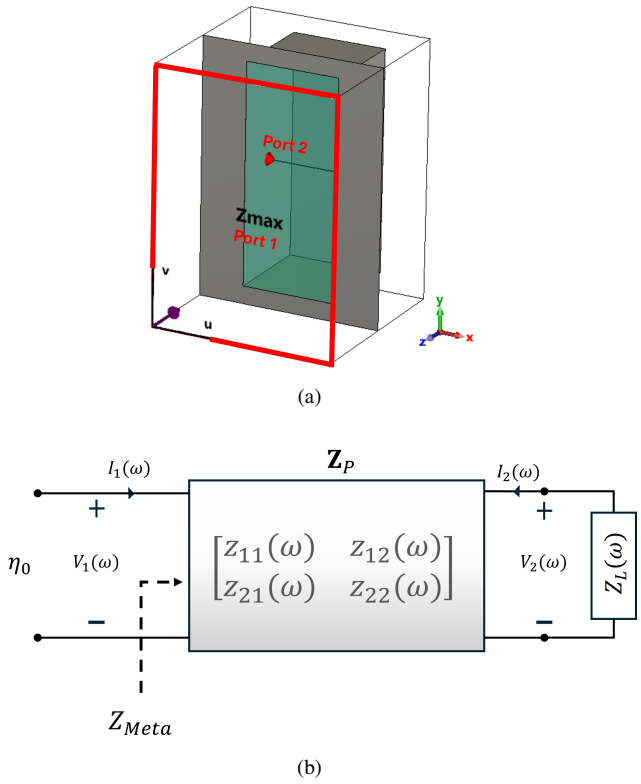

FIGURE 2. Illustration of the Macromodeling method with (a) the 2-port passive structure simulated in CST and (b) the network representation of the equivalent model for Γ calculation.

III. NUMERICAL RESULTS & DISCUSSION

Using both the FW CST solver and the Macromodeling technique of Section II-B, we performed unit cell characterization under different varactor loadings, whose results are reported in Fig. 4. In general, the reflection coefficients of the UC and its lookup table predicted by MM are in good agreement with CST, especially magnitude-wise, but in terms

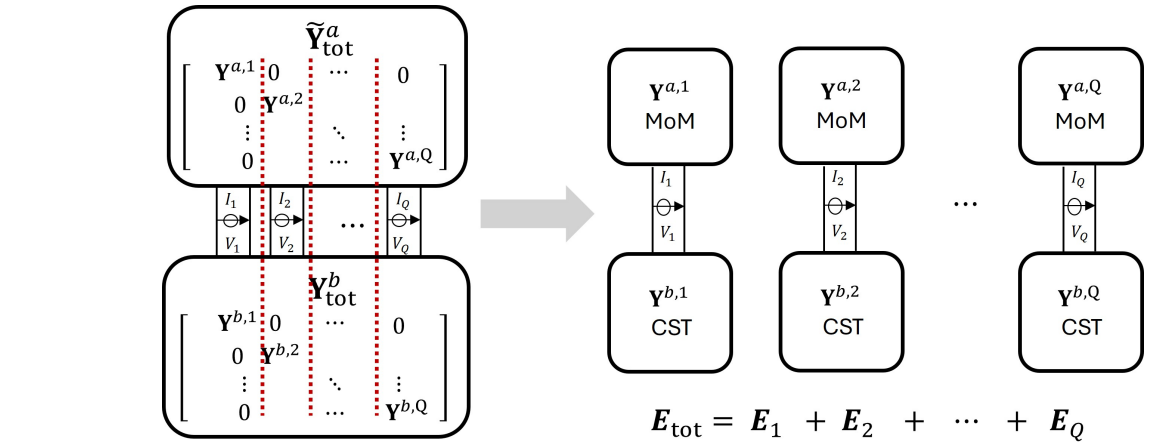

FIGURE 3. **The main idea behind the diagonalized admittance matrix in the framework of EIAP [16], which is implemented as a superposition of 1-element H-DDM problems.**

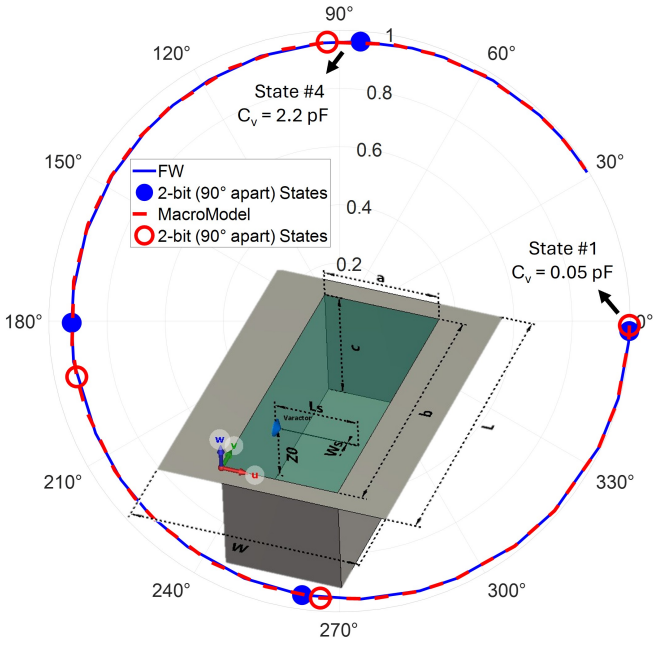

a	b	c	W	L	W_s	L_s	Z_0	ϵ_r	$\tan(\delta)$
9	21	9	17.6	24.3	0.05	6.5	4.5	3.5	0.0027

FIGURE 4. **Proposed unit cell's characterization and comparison of its so-called 'Look-up Table' predicted by MM vs FW CST simulations at the center frequency 0.85 GHz with C_v changing from 0.05 to 6 pF. Shown in the inset are also the UC dimensions (in cm) and the constitutive parameters of its dielectric filling (Polyimide).**

of phase, they slightly fall out of sync by either exhibiting some phase lead or lag, as shown for the 2-bit selected states in the figure. This is in agreement with our observations on MM's level of accuracy in UC characterization reported elsewhere [24].

At the panel level, it is both of great interest to the research community and one of the main contributions of this study to investigate how much over-the-air mutual coupling effects, neglected in EIAP, and the local periodicity assumption, used in MM, will cause the predictions to deviate from the reference or the 'ground truth' behavior of the panel. Note that in the lack of experimental measurements, FW analyses are used as the reference solutions throughout this study. To this end, several planar arrays composed of 4×4, 4×8, and 4×16 elements of the proposed unit cell have been designed and beamformed using the generalized law of reflection (GLR) [25] to reflect a normally incident plane wave onto a non-specular $30°$ elevation angle in the E-plane (X-Z plane). Since the lateral size of the proposed UC (W) is approximately half a free-space wavelength (λ_0) at the center frequency, GLR suggests a $-90°$ phase progression along $+x$ axis to achieve the desired reflection angle of $+30°$, corresponding to the four states $[0, -90, -180, -270]$ highlighted in Fig. 4 for varactor capacitance values of $0.05, 1.35, 1.625,$ and 2.2 pF, respectively.

Shown in Fig. 5 are the E-plane scattering patterns of these beamformed panels obtained using the algorithms discussed in Section II and compared against FW CST results serving as the reference solution in the absence of measurement results. For the sake of having a better visual comparison, both the linear and dB scales in Cartesian and polar coordinates are reported in the figure from which the following conclusions can be drawn:

- H-DDM and CST's integral equation (IE) solver show the closest agreement and are almost indistinguishable for the 4×4 and 4×8 cases as shown in Figs. 5a and 5c. For the 4×16 configuration, however, a proper mesh setting of the CST-IE solver put a stringent demand on our local server in terms of memory requirements and simulation run-time. Therefore, we were not able to simulate this case with CST's IE solver. Instead, we resorted to the default setting of the frequency domain (FD) solver of CST for this case whose result, shown in Fig. 5e in the E-plane and in Fig. 6 in 3D format, is still in close agreement with that of H-DDM but not

as close as the two smaller cases handled by CST's IE solver.

- As better emphasized in the polar coordinate sub-plots in Fig. 5, both MM and EIAP methods are good at predicting the main lobe direction, but they grow more and more inaccurate away from the main beam in their sidelobe predictions. It is important to notice that the nature and root cause of inaccuracies in these two approximate solutions are fundamentally different from one another. The discrepancies in EIAP's result stem from neglecting over-the-air mutual couplings among the cells in an otherwise identical implementation of H-DMM as described in detail in Section II-C. The inaccuracies in MM results, however, have their roots partly in the PBC assumption, whose impact shows up in the calculation of Γ_{mn} values under infinite periodic boundary conditions in Eq. (13) and partly from the pattern multiplication rule by incorporating the element pattern of one isolated meta-atom under a conjugate-matched loading condition.
- The results obtained from analyzing these types of panels composed of open-cavity based unit cells also indicate that neglecting only over-the-air mutual couplings in EIAP has less severe impact on the accuracy of the final results than the assumptions made through Macromodeling may result in. Nevertheless, as we also concluded in our previous work [24], MM as a viable and low-cost surrogate model can still serve well most of the applications that are mainly concerned about the main beam direction and can thus tolerate potential errors in their side-lobe predictions.

Finally, in an attempt to quantify the relative errors for the pattern prediction cases above, we calculated

$$\epsilon_{\text{Method}} = \left[\frac{1}{N_\theta}\sum_{l=1}^{N_\theta}\left|\frac{\text{Dir}^{\text{Method}}(\theta_l) - \text{Dir}^{\text{CST}}(\theta_l)}{\max\left(\text{Dir}^{\text{CST}}(\theta)\right)}\right|\right] \times 100\% \tag{15}$$

for each method and plotted them in Fig. 7, where N_θ is the total number of angular samples in the E-plane. The Algorithms' predictions tend to converge for bigger arrays although it should be noted that the jump in H-DDM from low error values for 32 elements (4×8 case) to higher ones for 64 elements (4×16 case) observed in the plot can be attributed primarily to the change of CST solver from IE to FD whose predicted main beam in Fig. 5f is now pointing to a slightly different direction than those predicted by the DDM-based methods.

IV. CONCLUSION

This work introduced a hybrid integral-equation domain decomposition method (H-DDM) tailored for accurate and efficient electromagnetic analysis of open-cavity-based RIS panels. The method was validated through benchmarking with CST full-wave solvers and compared against approximate approaches from the literature. Numerical results for beamformed RIS panels of different sizes demonstrate that H-DDM closely matches full-wave reference solutions across main-beam and sidelobe regions, whereas MM and EIAP exhibit noticeable discrepancies, particularly in sidelobe prediction. The analysis further reveals that neglecting only over-the-air mutual coupling in 1-element EIAP leads to less severe inaccuracies than the combined assumptions inherent to MM, especially the local periodicity and array factor approximations. Overall, the proposed H-DDM provides a computationally efficient tool for open-cavity based RISs. Future work will focus on extending the method to significantly reduce memory usage and runtime by incorporating several numerical acceleration strategies, including translational symmetry and adaptive cross approximation.

APPENDIX

To help the flow of the discussion throughout the paper, a brief overview of the basic formulation of DDM is provided here. To start with, the general compact operator formulas for electric and magnetic fields are as follows:

$$\boldsymbol{E} = \boldsymbol{E}(\boldsymbol{J}_s) + \boldsymbol{E}(\boldsymbol{M}_s) \quad \text{and} \quad \boldsymbol{H} = \boldsymbol{H}(\boldsymbol{J}_s) + \boldsymbol{H}(\boldsymbol{M}_s) \tag{16}$$

with the integro-differential operators given as

$$\boldsymbol{E}(\boldsymbol{J}_s) = \mathcal{L}(\boldsymbol{J}_s), \tag{17}$$

$$\boldsymbol{H}(\boldsymbol{M}_s) = \frac{1}{\eta^2}\mathcal{L}(\boldsymbol{M}_s) \tag{18}$$

and

$$\boldsymbol{E}(\boldsymbol{M}_s) = -\mathcal{K}(\boldsymbol{M}_s) + \frac{1}{2}\hat{\boldsymbol{n}} \times \boldsymbol{M}_s, \tag{19}$$

$$\boldsymbol{H}(\boldsymbol{J}_s) = \mathcal{K}(\boldsymbol{J}_s) - \frac{1}{2}\hat{\boldsymbol{n}} \times \boldsymbol{J}_s \tag{20}$$

where the operators $\mathcal{K}$ and $\mathcal{L}$ on any given input kernel $\boldsymbol{X}$ are defined as in [26]:

$$\mathcal{K}(\boldsymbol{X}_s) = \int_S \boldsymbol{X}_s(\boldsymbol{r}') \times \boldsymbol{\nabla}' G(\boldsymbol{r} - \boldsymbol{r}')\mathrm{d}S', \tag{21a}$$

$$\mathcal{L}(\boldsymbol{X}) = -j\omega\mu \int_S \boldsymbol{X}_s(\boldsymbol{r}')G(\boldsymbol{r} - \boldsymbol{r}')\mathrm{d}S' + \frac{1}{j\omega\varepsilon}\boldsymbol{\nabla}\int_S \boldsymbol{\nabla}' \cdot \boldsymbol{X}(\boldsymbol{r}')G(\boldsymbol{r} - \boldsymbol{r}')\mathrm{d}S'. \tag{21b}$$

Furthermore, the scalar Green's function for a homogeneous medium is

$$G(\boldsymbol{r} - \boldsymbol{r}') = \frac{e^{-jk|\boldsymbol{r}-\boldsymbol{r}'|}}{4\pi|\boldsymbol{r} - \boldsymbol{r}'|} = \frac{e^{-jkR}}{4\pi R}. \tag{22}$$

The wavenumber in the medium is given by its material constitutive parameters, i.e., $k^{a,b} = \omega\sqrt{\mu^{a,b}\varepsilon^{a,b}}$, and $\boldsymbol{r}'$ is a point in the source domain.

Enforcing continuity of tangential magnetic fields across the aperture as $\boldsymbol{H}^a_{\text{tan}} = \boldsymbol{H}^b_{\text{tan}}$ results in an MFIE formulation in which $\boldsymbol{H}^a$ has three contributors of firstly the form of impressed impinging wave from region a denoted as $\boldsymbol{H}^{a,i}$, secondly the form of magnetic field radiated by magnetic surface current $\boldsymbol{M}_s$ denoted as $\boldsymbol{H}^a(\boldsymbol{M}_s)$, and thirdly the form of magnetic field radiated by electric surface current

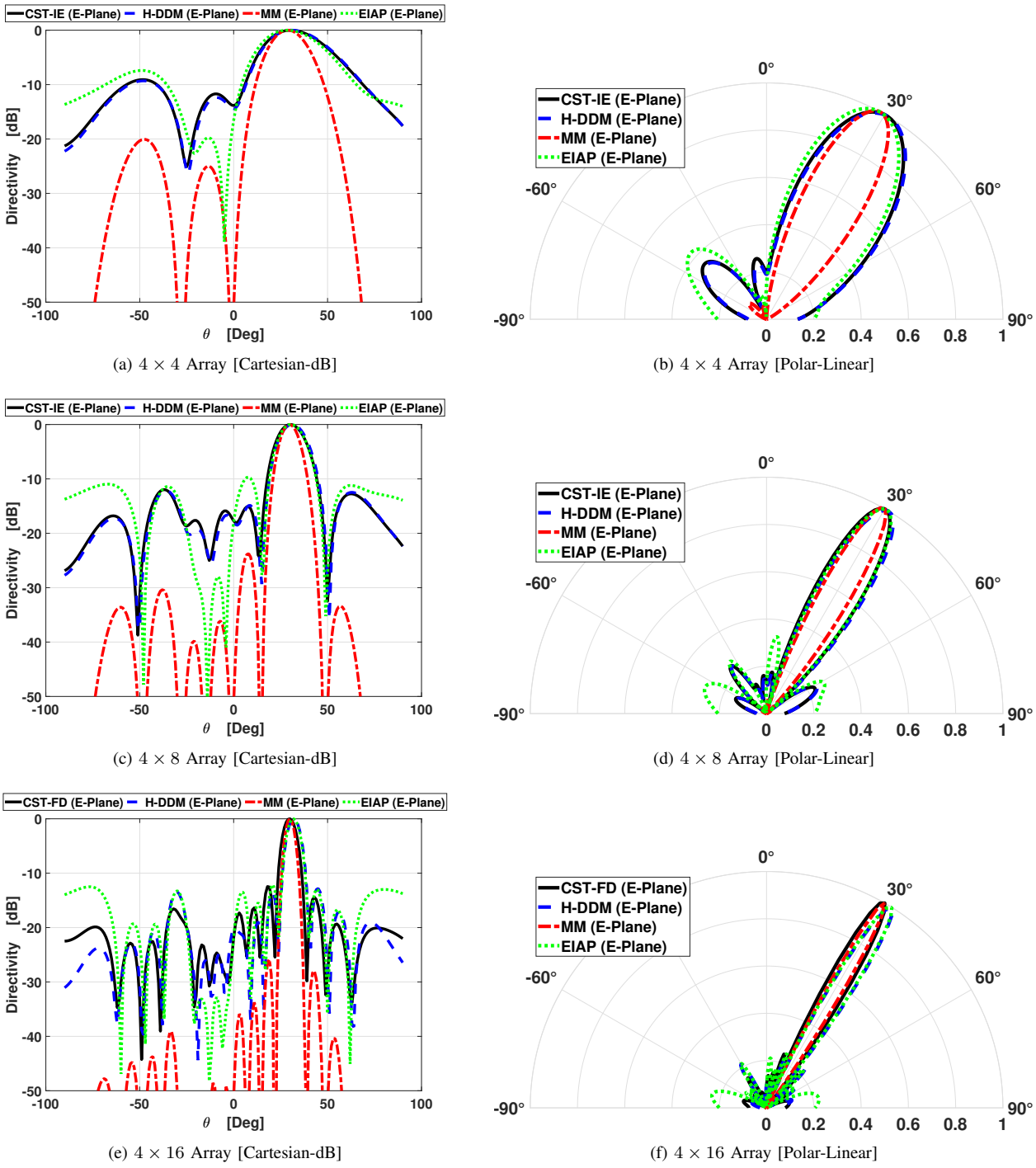

(a) 4×4 Array [Cartesian-dB]

(b) 4×4 Array [Polar-Linear]

(c) 4×8 Array [Cartesian-dB]

(d) 4×8 Array [Polar-Linear]

(e) 4×16 Array [Cartesian-dB]

(f) 4×16 Array [Polar-Linear]

FIGURE 5. Comparisons between the the four algorithms' predictions of E-plane FF-pattern cuts in Cartesian (first column) and polar (second column) coordinates for (a) and (b) 4×4, (c) and (d) 4×8, and (e) and (f) 4×16 arrays, all beamformed to reflect a normally incident plane wave onto the $+30^\circ$ elevation angle.

in region a denoted as $\boldsymbol{H}^a(\boldsymbol{J}_s^a)$. Note that $\boldsymbol{H}^b$ can be interpreted and constructed in a similar fashion just by replacing superscript a with b. With a bit of mathematical manipulation, we therefore have:

$$\Big[\boldsymbol{H}^a(\boldsymbol{M}_s) + \boldsymbol{H}^b(\boldsymbol{M}_s)\Big]_{\tan} + \Big[\boldsymbol{H}^a(\boldsymbol{J}_s^a) - \boldsymbol{H}^b(\boldsymbol{J}_s^b)\Big]_{\tan} = \Big[\boldsymbol{H}^{b,i} - \boldsymbol{H}^{a,i}\Big]_{\tan} \quad (23)$$

which is the exact MFIE equation at the aperture and can be cast into the framework of MoM and Galerkin weighted

This article has been accepted for publication in IEEE Open Journal of Antennas and Propagation. This is the author's version which has not been fully edited and content may change prior to final publication. Citation information: DOI 10.1109/OJAP.2026.3695418

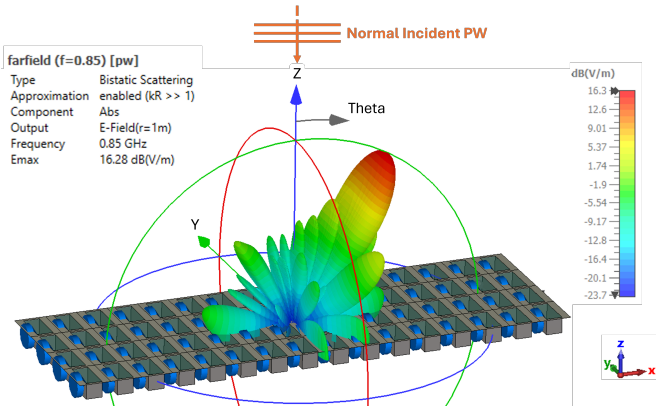

FIGURE 6. 3D CST FF-scattering pattern of the 4×16 panel beamformed to $+30^\circ$.

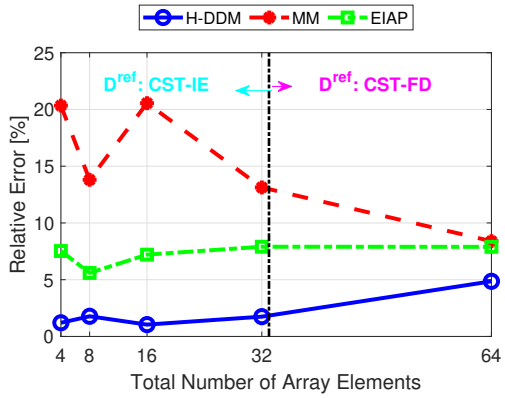

FIGURE 7. Pattern prediction errors of the investigated methods relative to the full-wave reference solution for 1×4, 1×8, 4×4, 4×8, and 4×16 array configurations.

residual approach:

$$\begin{aligned}&\langle -\boldsymbol{m}_m, \boldsymbol{H}^a_{\tan}(\boldsymbol{M}_s) + \boldsymbol{H}^b_{\tan}(\boldsymbol{M}_s)\rangle + \\ &\langle -\boldsymbol{m}_m, \boldsymbol{H}^a_{\tan}(\boldsymbol{J}^a_s) - \boldsymbol{H}^b_{\tan}(\boldsymbol{J}^b_s)\rangle \;=\\ &\langle -\boldsymbol{m}_m, \boldsymbol{H}^{b,i}_{\tan}\rangle - \langle -\boldsymbol{m}_m, \boldsymbol{H}^{a,i}_{\tan}\rangle, \quad m = 1, 2, \cdots, N\end{aligned} \tag{24}$$

Using linearity of the operators and the definition of aperture admittances, we obtain

$$\begin{aligned}&\sum_{n=1}^{N} \left[Y^a_{mn} + Y^b_{mn}\right] V_n + \sum_{n=1}^{N^b} C^b_{mn} I^b_n \\ &\quad - \sum_{n=1}^{N^a} C^a_{mn} I^a_n = I^{a,i}_m - I^{b,i}_m, \;\; m = 1, 2, \cdots, N\end{aligned} \tag{25}$$

where

$$Y^{a,b}_{mn} = -\frac{1}{\eta^2_{a,b}} \langle \boldsymbol{m}_m, \mathcal{L}^{a,b}(\boldsymbol{m}_n)\rangle \tag{26}$$

$$C^{a,b}_{mn} = \langle \boldsymbol{m}_m, \mathcal{K}^{a,b}(\boldsymbol{i}^{a,b}_n)\rangle - \frac{1}{2}\langle \boldsymbol{m}_m, \hat{\boldsymbol{n}}^{a,b} \times \boldsymbol{i}^{a,b}_n\rangle \tag{27}$$

$$I^{a,i}_m = \langle \boldsymbol{m}_m, \boldsymbol{H}^{a,i}_{\tan}\rangle \quad \text{and} \quad I^{b,i}_m = \langle \boldsymbol{m}_m, \boldsymbol{H}^{b,i}_{\tan}\rangle. \tag{28}$$

This set of N linear equations can be conveniently represented in the compact form of vector-matrix multiplication by rewriting Equation (25) as

$$\left[\mathbf{Y}^a + \mathbf{Y}^b\right] \mathbf{V} + \mathbf{C}^b \mathbf{I}^b - \mathbf{C}^a \mathbf{I}^a = \mathbf{I}^{a,i} - \mathbf{I}^{b,i}. \tag{29}$$

The ultimate goal is to find $\boldsymbol{M}_s$ of which $\mathbf{V}$ is an N-term variational approximate solution. In fact, $\mathbf{I}^a$ and $\mathbf{I}^b$ are intermediate, dependent variables and can therefore be found in terms of $\mathbf{V}$ by enforcing the second set of boundary conditions, i.e. ensuring electric field continuity at the aperture as follows:

$$\boldsymbol{E}^a_{\tan} = \hat{\boldsymbol{n}}^a \times \boldsymbol{M}_s = -\hat{\boldsymbol{n}}^b \times \boldsymbol{M}_s = \boldsymbol{E}^b_{\tan}, \tag{30}$$

which results in the two following EFIE equations

$$\left[\boldsymbol{E}^{a,i} + \boldsymbol{E}^a(\boldsymbol{M}_s) + \boldsymbol{E}^a(\boldsymbol{J}^a_s)\right]_{\tan} = \hat{\boldsymbol{n}}^a \times \boldsymbol{M}_s, \tag{31}$$

$$\left[\boldsymbol{E}^{b,i} - \boldsymbol{E}^b(\boldsymbol{M}_s) + \boldsymbol{E}^b(\boldsymbol{J}^b_s)\right]_{\tan} = -\hat{\boldsymbol{n}}^b \times \boldsymbol{M}_s. \tag{32}$$

Following a similar Galerkin procedure by testing with $\{\boldsymbol{i}^{a,b}_m\}$ and expansions to basis functions as before, the discretized version of the EFIEs read:

$$\sum_{n=1}^{N^a} Z^a_{mn} I^a_n = \sum_{n=1}^{N} D^a_{mn} V_n + V^{a,i}_m, \;\; \text{for } m = 1, \cdots, N^a$$

$$\sum_{n=1}^{N^b} Z^b_{mn} I^b_n = -\sum_{n=1}^{N} D^b_{mn} V_n + V^{b,i}_m, \;\; \text{for } m = 1, \cdots, N^b$$

where

$$Z^{a,b}_{mn} = -\langle \boldsymbol{i}^{a,b}_m, \mathcal{L}^{a,b}(\boldsymbol{i}^{a,b}_n)\rangle, \tag{33}$$

$$D^{a,b}_{mn} = -\langle \boldsymbol{i}^{a,b}_m, \mathcal{K}^{a,b}(\boldsymbol{m}_n)\rangle - \frac{1}{2}\langle \boldsymbol{i}^{a,b}_m, \hat{\boldsymbol{n}}^{a,b} \times \boldsymbol{m}_n\rangle \tag{34}$$

$$V^{a,i}_m = \langle \boldsymbol{i}^a_m, \boldsymbol{E}^{a,i}_{\tan}\rangle \quad \text{and} \quad V^{b,i}_m = \langle \boldsymbol{i}^b_m, \boldsymbol{E}^{b,i}_{\tan}\rangle, \tag{35}$$

or simply

$$\mathbf{Z}^a \mathbf{I}^a = \mathbf{D}^a \mathbf{V} + \mathbf{V}^{a,i} \tag{36a}$$

$$\mathbf{Z}^b \mathbf{I}^b = -\mathbf{D}^b \mathbf{V} + \mathbf{V}^{b,i}. \tag{36b}$$

By rearranging the above equations, the intermediate variables can now be expressed in terms of $\mathbf{V}$:

$$\mathbf{I}^a = \left(\mathbf{Z}^a\right)^{-1} \left(\mathbf{V}^{a,i} + \mathbf{D}^a \mathbf{V}\right), \tag{37a}$$

$$\mathbf{I}^b = \left(\mathbf{Z}^b\right)^{-1} \left(\mathbf{V}^{b,i} - \mathbf{D}^b \mathbf{V}\right) \tag{37b}$$

and finally, the substitution of $\mathbf{I}^a$ and $\mathbf{I}^b$ back into Equation (29) leads to the final generalized admittance formula given in (9).

ACKNOWLEDGMENT

This work was supported in part by the Advanced Digitalization program at the WiTECH Centre (DisCourSe & DigiArray projects), and in part by the SNS JU project Hexa-X-II (Grant Agreement No. 101095759) under the EU's Horizon Europe Research and Innovation Programme.

REFERENCES

[1] C. L. Holloway, E. F. Kuester, J. A. Gordon, J. O'Hara, J. Booth, and D. R. Smith, "An overview of the theory and applications of metasurfaces: The two-dimensional equivalents of metamaterials," *IEEE Antennas Propag. Mag.*, vol. 54, no. 2, pp. 10–35, 2012.

[2] J. C. Liang, Q. Cheng, Y. Gao, C. Xiao, S. Gao, L. Zhang, S. Jin, and T. J. Cui, "An angle-insensitive 3-bit reconfigurable intelligent surface," *IEEE Trans. Antennas Propag.*, vol. 70, no. 10, pp. 8798–8808, 2021.

[3] Y. Liu, X. Liu, X. Mu, T. Hou, J. Xu, M. Di Renzo, and N. Al-Dhahir, "Reconfigurable intelligent surfaces: Principles and opportunities," *IEEE Commun. Surveys Tuts.*, vol. 23, no. 3, pp. 1546–1577, 2021.

[4] J. Sang, Y. Yuan, W. Tang, Y. Li, X. Li, S. Jin, Q. Cheng, and T. J. Cui, "Coverage enhancement by deploying ris in 5g commercial mobile networks: Field trials," *IEEE Wirel. Commun.*, vol. 31, no. 1, pp. 172–180, 2022.

[5] M. Jiang, W. J. Ran, J. W. Wu, X. Yang, Y. Li, R. Y. Wu, Q. Cheng, J. Hu, and T. J. Cui, "Efficient and accurate simulations of metamaterials based on domain decomposition and unit feature database," *IEEE Trans. Antennas Propag.*, 2024.

[6] W. Tang, M. Z. Chen, X. Chen, J. Y. Dai, Y. Han, M. Di Renzo, Y. Zeng, S. Jin, Q. Cheng, and T. J. Cui, "Wireless communications with reconfigurable intelligent surface: Path loss modeling and experimental measurement," *IEEE Trans. Wireless Commun.*, vol. 20, no. 1, pp. 421–439, 2020.

[7] Ö. Özdogan, E. Björnson, and E. G. Larsson, "Intelligent reflecting surfaces: Physics, propagation, and pathloss modeling," *IEEE Wirel. Commun. Lett.*, vol. 9, no. 5, pp. 581–585, 2019.

[8] F. Costa and M. Borgese, "Electromagnetic model of reflective intelligent surfaces," *IEEE Open J. Commun. Soc.*, vol. 2, pp. 1577–1589, 2021.

[9] Z. Zhang, J. W. Zhang, J. W. Wu, J. C. Liang, Z. X. Wang, Q. Cheng, Q. S. Cheng, T. J. Cui, H. Q. Yang, G. B. Liu *et al.*, "Macromodeling of reconfigurable intelligent surface based on microwave network theory," *IEEE Trans. Antennas Propag.*, vol. 70, no. 10, pp. 8707–8717, 2022.

[10] J. W. Zhang, Z. Zhang, J. Zhang, J. W. Wu, J. Y. Dai, Q. Cheng, Q. S. Cheng, and T. J. Cui, "A novel two-stage optimization framework for designing active metasurfaces based on multiport microwave network theory," *IEEE Trans. Antennas Propag.*, vol. 72, no. 2, pp. 1603–1616, 2023.

[11] M. A. Francavilla, E. Martini, S. Maci, and G. Vecchi, "On the numerical simulation of metasurfaces with impedance boundary condition integral equations," *IEEE Trans. Antennas Propag.*, vol. 63, no. 5, pp. 2153–2161, 2015.

[12] Y. Vahabzadeh, K. Achouri, and C. Caloz, "Simulation of metasurfaces in finite difference techniques," *IEEE Trans. Antennas Propag.*, vol. 64, no. 11, pp. 4753–4759, 2016.

[13] I. Bardi, R. Remski, D. Perry, and Z. Cendes, "Plane wave scattering from frequency-selective surfaces by the finite-element method," *IEEE Trans. Magn.*, vol. 38, no. 2, pp. 641–644, 2002.

[14] J. Budhu and A. Grbic, "Perfectly reflecting metasurface reflectarrays: Mutual coupling modeling between unique elements through homogenization," *IEEE Trans. Antennas Propag.*, vol. 69, no. 1, pp. 122–134, 2020.

[15] R. Maaskant, D. Lin, F. Maxharraj, M. Ghaderi Aram, L. Manholm, P. Aghdam, G. Gerini, T. Svensson, and M. Ivashina, "Domain decomposition analysis of open-cavity-based array elements - roadmap toward analyzing large-scale reflectarrays and reconfigurable intelligent surfaces," in *Proc. Int. Conf. Electromagn. Adv. Appl. (ICEAA)*, 2025, pp. 687–692.

[16] H. Li, B.-Z. Wang, L. Guo, W. Shaoand, and P. Du, "A far field pattern analysis technique for reflectarrays including mutual coupling between elements," *J. Electromagn. Waves Appl.*, vol. 23, no. 1, pp. 87–95, 2009.

[17] Y. Ma, J. F. Kolb, A. A. Ihalage, A. S. Andy, and Y. Hao, "Incorporating meta-atom interactions in rapid optimization of large-scale disordered metasurfaces based on deep interactive learning," *Adv. Photon. Res.*, vol. 4, no. 4, p. 2200099, 2023.

[18] G. Xu, S. V. Hum, and G. V. Eleftheriades, "Augmented huygens' metasurfaces employing baffles for precise control of wave transformations," *IEEE Trans. Antennas Propag.*, vol. 67, no. 11, pp. 6935–6946, 2019.

[19] R. F. Harrington and J. R. Mautz, "Electromagnetic coupling through apertures by the generalized admittance approach," *Comput. Phys. Commun.*, vol. 68, no. 1-3, pp. 19–42, 1991.

[20] S. Rao, D. Wilton, and A. Glisson, "Electromagnetic scattering by surfaces of arbitrary shape," *IEEE Trans. Antennas Propag.*, vol. 30, no. 3, pp. 409–418, 1982.

[21] R. Harrington, *Time-Harmonic Electromagnetic Fields*, ser. IEEE Press Ser. Electromagn. Wave Theory. Wiley, 2001.

[22] R. Maaskant and M. Arts, "Reconsidering the voltage-gap source model used in moment methods," *IEEE Antennas Propag. Mag.*, vol. 52, no. 2, pp. 120–125, 2010.

[23] C. A. Balanis, *Antenna theory: analysis and design*. John wiley & sons, 2016.

[24] M. Ghaderi Aram, F. Maxharraj, R. Maaskant, and T. Svensson, "On RIS Macromodeling of a Large Holographic-Inspired Beamforming Panel," in *2026 20th European Conference on Antennas and Propagation (EuCAP)*. IEEE, 2026, accepted; to appear.

[25] N. Yu, P. Genevet, M. A. Kats, F. Aieta, J.-P. Tetienne, F. Capasso, and Z. Gaburro, "Light propagation with phase discontinuities: generalized laws of reflection and refraction," *science*, vol. 334, no. 6054, pp. 333–337, 2011.

[26] W. C. Gibson, *The method of moments in electromagnetics*. Chapman and Hall/CRC, 2021.

MORTEZA GHADERI ARAM (Graduate Student Member, IEEE) was born in Hamedan, Iran, in 1988. He received the B.Sc. degree in electrical engineering – Bioelectric from Sahand University of Technology, Tabriz, Iran, in 2011, the M.Sc. degree in Telecommunications – Fields & Waves from K. N. Toosi University of Technology, Tehran, Iran, in 2015, and the Licentiate degree in Bio-electromagnetics from Chalmers University of Technology, Gothenburg, Sweden, in 2022. He is currently pursuing the Ph.D. degree in Telecommunications – Antenna Systems with the electrical engineering department of Chalmers University of Technology.

From 2023 to 2024, he was a Project Assistant with the Wireless Systems Lab of Chalmers, where he was involved in the development of a digital twin platform for 6G wireless networks. His research interests include applied and computational Electromagnetics, Metasurfaces, smart antennas for mobile and satellite communications, Holographic MIMO, EM-compliant channel modeling, inverse scattering, and non-destructive microwave sensing and imaging.

Mr. Ghaderi Aram was a recipient of the 3rd Annual ESHO Sensius Young Investigators Award in 2019 and the Chalmerska Forskningsfonden Grant in 2020. He was a member of the organizing committee for the Swedish Communication Technologies Workshop (Swe-CTW) in 2024, and since 2020 has served as a reviewer for a number of technical journals in the field including *IEEE Transactions on Antennas and Propagation*, *Applied Physics Letters*, and *IEEE Journal of Electromagnetics, RF and Microwaves in Medicine and Biology*.

TOMMY SVENSSON (Senior Member, IEEE) is Full Professor in Communication Systems at Chalmers University of Technology in Gothenburg, Sweden, where he is leading the Wireless Systems research on air interface and wireless backhaul networking technologies for future wireless systems. He received a Ph.D. in Information theory from Chalmers in 2003, and he has worked at Ericsson AB with core networks, radio access networks, and microwave transmission products.

He was involved in the European WINNER I/II/+ and ARTIST4G projects that made important contributions to the 3GPP LTE standards, the EU FP7 METIS and the EU H2020 5GPPP mmMAGIC and 5GCar projects towards 5G, and the Hexa-X-I/II, RISE-6G, SEMANTIC, ROBUST-6G and ECO-eNET projects towards 6G, as well as in the ChaseOn/Bridge Center/emerging WiTECH antenna systems excellence centers at Chalmers targeting mm-wave and (sub)-THz solutions for 5G/6G access, backhaul/ fronthaul and V2X scenarios.

His main research interests are in design and analysis of mobile communication systems, physical layer algorithms, multiple access, resource allocation, cooperative/ situational-aware communications, mm-wave/ sub-THz communications, C-V2X, ISAC, physical-layer security, non-terrestrial-networks, sustainable design, end-to-end architecture. He has co-authored 7 books, 150 journal papers, 180 conference papers, and 80 public EU projects deliverables. He is founding editorial board member and editor of IEEE JSAC Series on Machine Learning in Communications and Networks, has been Chairman of the awards winning IEEE Sweden joint Vehicular Technology/ Communications/ Information Theory Societies chapter, editor of IEEE Transactions on Wireless Communications, IEEE Wireless Communications Letters, Guest editor of several top journals, organized several tutorials and workshops at top IEEE conferences, Lead local organizer of EuCNC & 6G Summit 2023, and served as coordinator of the Communication Engineering Master's Program at Chalmers. Since 2022 he is board member of Swedish telecommunications regulator PTS.

FITIM MAXHARRAJ (Graduate Student Member, IEEE) received the B.Sc. degree in electrical engineering and the M.Sc. degree in wireless, photonic, and space engineering from Chalmers University of Technology, Gothenburg, Sweden.

He is currently pursuing the Ph.D. degree with the Antenna Group, Department of Electrical Engineering, Chalmers University of Technology.

His research interests include fast analysis and design methods for large reconfigurable reflectarrays and intelligent surfaces (RIS).

ROB MAASKANT (Senior Member, IEEE) received the M.Sc. and Ph.D. degrees (both *cum laude*) in electrical engineering from the Eindhoven University of Technology (TU/e), Eindhoven, The Netherlands, in 2003 and 2010, respectively.

From 2002 to 2010, he was with the Netherlands Institute for Radio Astronomy (ASTRON), Dwingeloo, The Netherlands, where he worked as an Antenna Researcher. Since 2010, he has been with the Antenna Group, Department of Electrical Engineering, Chalmers University of Technology, Gothenburg, Sweden, where he is currently a Professor.

He has held prestigious research fellowships and grants, including a Marie Skłodowska-Curie Fellowship (Rubicon, NWO), and faculty positions at both TU/e and Chalmers supported by competitive funding programs. He is the primary developer of the CAESAR software, an advanced integral-equation-based solver for the analysis of large-scale antenna array systems. His research focuses on the analysis and design of integrated antenna systems, including reconfigurable intelligent surfaces (RIS) and full-duplex integrated sensing and communication (ISAC) for next-generation wireless systems.

Dr. Maaskant has served the antennas and propagation community as an Associate Editor for the *IEEE Transactions on Antennas and Propagation*, the *IEEE Antennas and Wireless Propagation Letters*, and the *Forum for Electromagnetic Research Methods and Application Technologies* (FERMAT).